Selective Elasticity Data Acquisition on 3D Deformable Objects for Virtualized Reality Applications

Ana-Maria Cretu, Pierre Payeur and Emil M. Petriu

Abstract—**This paper proposes the use of self-organizing architectures, particularly the growing neural gas, for the purpose of automatically guiding elasticity data acquisition based on a sparse vision and elasticity point-cloud of a 3D object. The proposed solution allows for the identification of regions where changes in the elastic behavior of the object occur. Additional data can then be collected in these areas in order to better characterize the elastic characteristics of a certain object. Experimental results for different non-homogeneous objects are presented in order to validate the proposed solution.**

I. Introduction

MUCH of the current research effort is directed towards means to deal with the computational cost of increasingly complex models and the requirements for real-time interaction with computer-generated deformable models. Often, these time constraints lead to simplifications in the modeling of deformable objects such that the computer model exhibits only some degree of physically plausible dynamic behavior. Elastic parameters are chosen according to some *a priori* knowledge on the deformable object model. Alternatively, the user has the choice to set the values of the elastic parameters following a subjective comparison between the perceived appearance or tactile feeling that he/she experiences when interacting with both the real object and a computer generated model of the same object. This procedure can result in endless trials and errors when a certain degree of realism is required. While such approaches can be employed for certain types of applications that do not necessarily require physically-correct deformable models, they cannot be employed where accuracy is expected.

There are relatively few publications reporting any sort of actual elasticity measurements for the development of virtualized reality applications. This is justified by the complex procedures involved in the capture and measurement of elastic behavior. The results obtained during measurements are often difficult to interpret as long as no assumptions are made on the material of the object under study, and the modeling of elastic behavior poses additional challenges.

In those cases where measurements are collected, often a single probing of the object is performed to elicit the elastic behavior, or some samples are collected randomly over the surface of the object under study. Such probing procedures are inappropriate for heterogeneous or piecewise homogeneous objects that have varying elasticity in different parts of their bodies as they could miss essential information regarding the elastic characteristics of the objects. Moreover, the procedure to collect experimental elastic data is still much more time consuming than similar procedures to gather vision data. These aspects explain the considerable interest in finding fast, automatic sampling procedures for the measurement of the elastic properties of 3D object surfaces. Appropriate elasticity data acquisition procedures should be able to minimize the number of the sampled points by selecting only those points that are representative of the elastic characteristics, or changes thereof, over an object.

II. Literature Review

The interest on the topic of probing objects in order to elicit their elastic properties being relatively recent, very few papers have yet been published on the subject. D'Aulignac *et al.* [1] employ uniform sampling of human thigh to elicit its elastic behaviour. A probe mounted on a force sensor and on a robot arm, positioned perpendicularly to the surface of a human thigh is employed to collect measurements, distributed regularly over the surface. The model parameters are then estimated using an optimization approach based on nonlinear least squares estimation. Uniform sampling offers a straightforward solution to ensure complete coverage of the surface within the region of interest. However in order to achieve adequate sampling density over those regions where elasticity is more likely to vary, the sampling density must be uniformly high over the entire surface, which may lead to inefficiency that is compromising certain applications.

Pai *et al.* [2, 3] use a probing procedure that considers a known surface mesh of the object and a predefined set of parameters (e.g. the maximum force exerted on the object, the maximum probing depth, and the number of steps for the deformation measurement). During probing, the designed algorithm generates the next position and orientation for the probe based on the specified parameters and the mesh of the object under test. It performs at the same time proximity checks and verifies the expected contact location of the probe with the mesh based on line intersection. The

This work was supported in part by the Communications and Information Technology Ontario Centre of Excellence and the Natural Sciences and Engineering Research Council of Canada

Ana-Maria Cretu is with the School of Information Technology and Engineering, University of Ottawa, 800 King Edward, Ottawa, Ontario, K1N 6N5, Canada (phone: 613-562-5800; fax: 613-562-5664; e-mail: acretu@ site.uottawa.ca).

Pierre Payeur is with the School of Information Technology and Engineering, University of Ottawa, 800 King Edward, Ottawa, Ontario, K1N 6N5, Canada (e-mail: ppayeur@ site.uottawa.ca).

Emil M. Petriu is with the School of Information Technology and Engineering, University of Ottawa, 800 King Edward, Ottawa, Ontario, K1N 6N5, Canada (e-mail: petriu@ site.uottawa.ca).

procedure is adaptive in that it adjusts itself to the results of the interaction with the object. However, the probing procedure is not selective, as it can involve the collection of data for all the points over the mesh, and therefore can reach very long acquisition time.

The work presented in this paper is a continuation of the research that we performed on the topic of selective probing of 3D objects properties [4-7]. An adaptation of a solution originally developed in the context of vision sampling [5, 6] is performed in order to identify areas of change in the elastic behavior of objects.

III. Proposed Framework

The elasticity data acquisition framework proposed here is meant to guide the automated selection of regions of interest for the characterization of the elastic behavior of an object, in order to obtain a more accurate description of its elastic characteristics. The proposed solution is presented in Fig. 1.

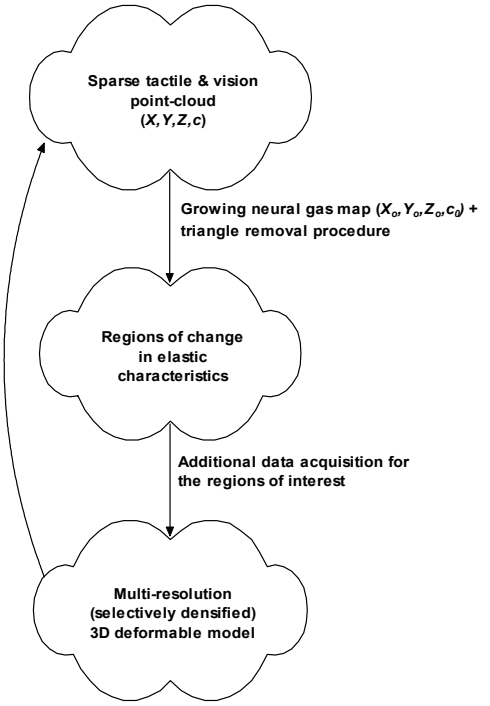

Fig. 1. Proposed framework for selective elasticity data acquisition.

Starting from an initial sparse elasticity and geometric surface scan over a 3D object, that is rapidly acquired, a growing neural gas is employed to cluster measurements that represent uniform elasticity regions and therefore direct the tactile sensor toward areas of transitions where higher sampling density is required. The growing neural gas is chosen since it revealed to be faster, to lead to lower errors in mapping and to require less user interaction in the modeling procedure [6].

Those regions that are worth further sampling in order to ensure an accurate model of elasticity are detected by finding areas in the growing neural gas map where changes in elastic behavior occur. Rescanning at higher resolution is performed for each identified region and a multi-resolution 3D deformable model is then built by augmenting the initial sparse model with the higher resolution data collected only over the regions of interest. If a more compact model is desired, the growing neural gas map can be augmented with the higher resolution areas as well.

A. Growing Neural Gas Networks

Growing neural gas is an unsupervised incremental clustering algorithm, whose purpose is to generate a graph structure that reflects the topology of the input data manifold [8]. This topology is generated using competitive Hebbian learning [9], which inserts an edge between the two closest nodes. The closeness is measured in Euclidian distance from an input vector. There are no restrictions on the topology. Arbitrary edges are allowed and the topology can have different dimensionalities in different parts of the input space. The resulting graph is an induced Delaunay triangulation. This induced Delaunay triangulation has been shown to optimally preserve topology in a very general sense [9].

The growing neural gas algorithm can be described as follows: new nodes are added every λ iterations, to support the node with the highest local accumulated error. For each input vector presented to the network, two best matching nodes are selected, whose weights are the closest to the input, based on Euclidean distance. A neighborhood connection is created between them if the connection does not already exist and its age is set to 0. The position of these nodes and the ones of the topological neighbors of the winner unit are moved such that they better fit the input. All edges that are not used increase in age and if the age exceeds a threshold (a_{max}), the corresponding edges are deleted. Any node that has no edge connection is removed as well. After λ iterations, a new node is added to support the node that has accumulated the highest error in the previous steps. The new node is placed between the node with the highest error and one of its neighbors that has the next highest error in order to ensure the minimization of their future errors. The algorithm continues until some stopping criterion is met.

The growing neural gas algorithm can be described formally as follows [8, 10]:

1. The network is initialized with two units c_1 and c_2:

$$S = \{c_1, c_2\} \tag{1}$$

with the corresponding reference vectors $w_{c_1}, w_{c_2} \in \Re^n$ (each unit c has an associated n-dimensional reference vector that indicates its position in the input space) chosen randomly according to a probability density function $p(x)$ or chosen from a finite set $D = \{x_1, x_2, ..., x_M \mid x_i \in \Re^n\}$ and the connection set, C, is initialized to the empty set.

$$C \subset S \times S,\ C = \phi \tag{2}$$

The set C is a set of un-weighted and symmetric neighborhood connections, used for the adaptation of the winner and its topological neighbors.

2. A random input vector x is generated based on p(x) or chosen from a finite set D and presented to the network.

3. The winner and second-nearest units $s_1, s_2 \in S$ are determined by:

$$s_1 = \arg\min_{c \in S} \|x - w_c\| \quad (3)$$

and

$$s_2 = \arg\min_{c \in S \setminus \{s_1\}} \|x - w_c\| \quad (4)$$

4. If s_1 are s_2 are not connected, a connection is created and added to the connection set:

$$C = C \cup \{s_1, s_2\} \quad (5)$$

and the age of the connection between them is set to 0.

$$age(s_1, s_2) = 0 \quad (6)$$

5. The squared distance between the input signal and the winner is added to a local error variable:

$$\Delta E_{s_1} = \|x - w_{s_1}\|^2 \quad (7)$$

6. The reference vectors of the winner and its direct topological neighbors are adapted by fractions ε_b and ε_n respectively of the distance to the input signal:

$$\Delta w_{s_1} = \varepsilon_b (x - w_{s_1}) \quad (8)$$

$$\Delta w_{s_i} = \varepsilon_n (x - w_{s_{i1}}), \forall i \in N_{s_1} \quad (9)$$

where N_{s_1} is the set of direct topological neighbors of s_1.

7. The ages of all edges emanating from s_1 are incremented by 1:

$$age(s_1, i) = age(s_1, i) + 1, \forall i \in N_{s_1} \quad (10)$$

8. All edges with the age larger than a_{max} are removed. If this results in units having no more emanating edges, those units are removed as well.

9. If the number of the input signals generated so far is an integer multiple of λ, then a new unit is inserted as follows:

a) Determine the unit q with maximum accumulated error:

$$q = \arg\max_{c \in S} E_c \quad (11)$$

b) Determine the unit f among the neighbors of q with the maximum accumulated error:

$$f = \arg\max_{c \in N_q} E_c \quad (12)$$

c) Add a new unit r to the network and interpolate its reference vector for q and f.

$$S = S \cup \{r\}, \quad w_r = (w_q + w_f)/2 \quad (13)$$

d) Insert edges connecting q and f with r and remove the original connection between q and f:

$$C = C \cup \{(r, q), (r, f)\}, \qquad C = C \setminus \{(q, f)\} \quad (14)$$

e) Decrease the error variables of q and f by a fraction α:

$$\Delta E_q = -\alpha E_q, \qquad \Delta E_f = -\alpha E_f \quad (15)$$

f) Interpolate the error variable of r from the ones of q and f:

$$E_r = (E_q + E_f)/2 \quad (16)$$

10. The error of all units is decreased:

$$\Delta E_c = -\beta E_c, \quad \forall c \in S \quad (17)$$

11. If a stopping criterion is not met, return to step 2.

One of the main advantages of growing neural gas is the fact that its parameters are constant [8, 10]. During the experiments, the parameters are set, as suggested in the literature, to: ε_b=0.05, ε_n=0.0006, α=0.5, β=0.0005 and the values for the number of iterations after a node is inserted and the age threshold are set as: λ=3 and a_{max}=20.

B. Selection of Regions with Changing Elasticity

The growing neural gas has the ability to find an optimal finite set that quantizes the given input space. Starting from an initial vision and tactile sparse scan, the proposed solution identifies those regions that are representative for the elastic characteristics of objects in order to ensure the capability of the application to deal not only with homogeneous objects from the elasticity point of view, but also with non-homogeneous, particularly piecewise-homogeneous objects.

The input space of the growing neural gas is composed of four dimensional vectors in the form of (*X, Y, Z, c*), where (*X,Y,Z*) are the geometric coordinates of a point obtained during the sparse/fast scan using a laser 3D scanner [6, 7], and *c* is a measure of elasticity at that point, as will be further discussed. The addition of this parameter to the parametric space enhances the behavior of the proposed framework for objects where changes in the elastic behavior are not correlated with variations in the local geometry of the surface.

A Delaunay triangulation is applied on the (X_o, Y_o, Z_o) (identified in Fig. 1) coordinates of points contained in the growing neural gas map after adaptation. In order to identify areas where changes in elastic behavior occur, triangles are subsequently removed from this triangulation of the output map of the growing neural gas [7] based on two criteria. First, a threshold is automatically computed based on the length of vertices for every triangle in the tessellation. The procedure of removing triangles with edges longer than the threshold identifies areas where a high density of nodes

occurs in the output map. Such high-density regions identify changes in the local geometry. The procedure therefore allows for a better characterization of those changes in the elastic behavior that are correlated to changes in the geometry. Second, triangles are also removed where the three vertices of a given triangle have the same elasticity measure, *c*, representing local uniformity in the elasticity properties. Only triangles that have different elasticity measures for one or two of their vertices are preserved, therefore identifying the areas where changes in the elastic characteristics occur.

Rescanning at higher resolution is then performed for every identified region (regions marked by the remainder of triangles in the tessellation) and a multi-resolution 3D deformable model is finally built by augmenting the initial sparse model with the high resolution geometric and elasticity data collected over the regions of interest.

IV. Experimental Results

The set of deformable objects used for testing are depicted in Fig. 2: a pair of pliers, a plastic bottle and a toy triceratops. These are all examples of objects made of non-homogeneous or piecewise homogeneous elastic materials.

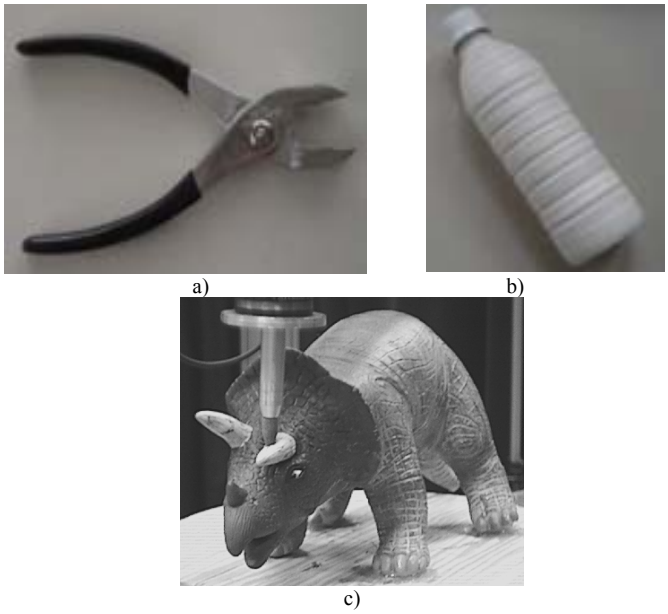

a) b) c)

Fig. 2. Deformable objects used for testing: a) pair of pliers, b) plastic bottle, and c) toy triceratops.

The procedure starts by collecting data samples, both geometric and elastic over the surface of the object. The geometric data is collected using a scan-line laser sensor. The equipment and procedures are described in detail in [5]. Elastic data is collected either in the form of deformation profiles [6] at each of the sparse model points (pliers and bottle) or in the form of force-displacement curves over time at each vertex of the mesh [4] (for the toy triceratops), using in both cases a force-torque sensor.

A simplistic measure of elasticity can be obtained from force-displacement curves: i.e. estimating the compliance at each probed point. The compliance is the inverse of stiffness which is a measure of the resistance of an object's body to the deformation resulting from applying an external force. It corresponds to a constant ratio between force and displacement, similar to the behavior of a linear elastic material under small deformation, or of a linear spring, and it can be obtained by approximating a measured force-displacement curve (as depicted in Fig. 3a) by a straight line [4].

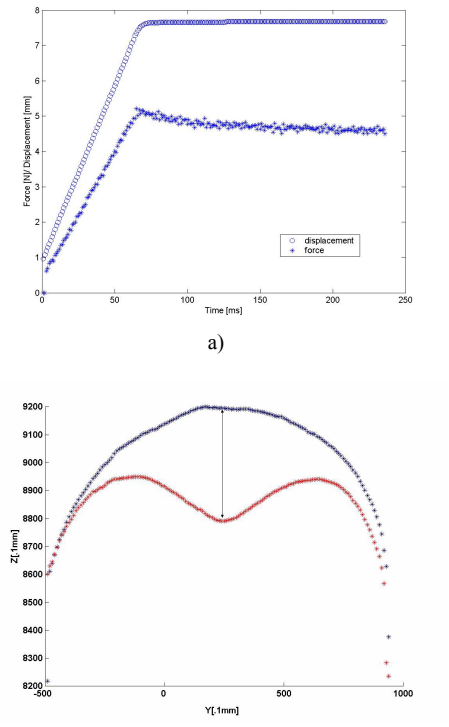

a)

b)

Fig. 3. a) Force-displacement curve at a vertex of the triceratops model, and b) deformation profiles associated with force measurements for the plastic bottle.

In the case of the deformation profiles, it is impossible to compute explicitly the stiffness, since there is no explicit value for the displacement available. However, a measure of the displacement and therefore of the elastic behavior can be computed by comparing the deformation profiles when no force is acting on the object and while a force acts on a point of an object, as shown in Fig. 3b for the case of the plastic bottle. Fig. 3b shows in blue the non-deformed profile of the plastic bottle prior to any interaction with the force sensor, and in red the deformation profile when a force is applied on the bottle. The point where the force acts can be determined by computing the difference vector between the two profiles and looking for the largest component of this vector. This largest component can be considered as a measure of displacement at the interaction point. The compliance is then computed as the ratio between the displacement and the force acting on the object that causes the displacement, and its average value is stored for each measured point.

The *(X, Y, Z)* geometric coordinates of each point in the surface profile together with the corresponding compliance are used as an input to the growing neural gas. Normalization is employed to remove redundant information

from the data set, by performing a linear rescaling of the input vectors such that their variance is 1.

Fig. 4 to Fig. 6 show results of the application of the proposed framework for the three objects considered, with different regions of elastic behavior depicted in different colors.

The point-cloud for a pair of pliers is depicted in Fig. 4a. The plastic handle has different elasticity characteristics than the peak (the peak, in metal is denoted by a lighter blue shade; the handle, in plastic, that is slightly smoother, is shown in darker blue shade).

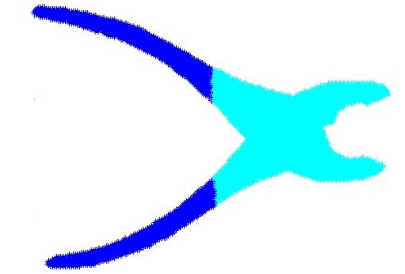

a)

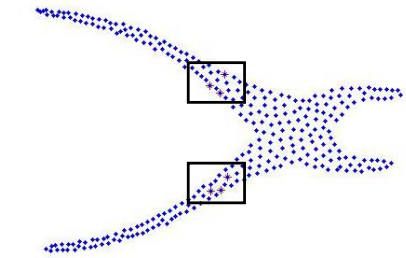

b)

Fig. 4. (a) Initial scan of the pliers with compliance information, and (b) growing neural gas model with detected regions of interest selected for further probing.

The growing neural gas map is depicted in Fig. 4b with the vertices of triangles remaining after the triangle removal procedure, as explained in section III.B, marked with stars inside the two bounding boxes. Areas containing these points are identified as areas of interest for additional data acquisition in order to better characterize the transition line between the regions of different elasticity properties.

The case of the plastic bottle is illustrated in Fig. 5. As in the case of the pliers, the bottle is composed from the elasticity point of view of two parts with different elastic behaviors: the bottle cap (rigid plastic material, depicted in red) and the bottle body (deformable plastic material, depicted in blue). Fig. 5b denotes the growing neural gas map with compliance shown in color. Fig. 5c shows the vertices of triangles that were preserved after the removal procedure, overlapped on the growing neural gas output. The corresponding area identified for additional probing is delimited with a rectangular bounding box. In both of the presented cases the proposed procedure identifies precisely those areas where changes in elastic behavior occur.

a)

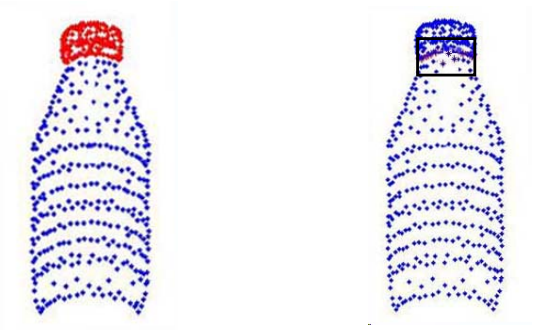

b) c)

Fig. 5. (a) Initial scan of bottle with compliance information, b) growing neural gas model of bottle with compliance, and (c) detected areas for additional elasticity measurements.

The results for the triceratops are shown in Fig. 6. Fig. 6a shows the sparse scan with compliance used as input for the growing neural gas map. The sparse scan considered contains 6113 points and has been obtained by subsampling a full resolution scan containing 65536 points, that was obtained with a different technology and made available for this experimentation [3]. The growing neural gas output map of 2562 points is depicted in Fig. 6b. It can be seen that the model preserves very well the compliance information.

The vertices of those triangles that are left after the removal procedure as explained in section III.B are marked with red stars over the growing neural gas map in Fig. 6c. It can be seen that all the areas where changes in the elastic characteristics occur are correctly identified using the proposed framework. It can also be observed however that the area in the tail of the triceratops which exhibits different elastic behaviors, depicted in light blue, is not fully captured in the map. A partial correction of this error can be done by the rescanning of a slightly larger area around the detected red star marks. The resulting areas where additional data acquisition is suitable are indicated with rectangles in Fig. 6d. Slightly larger rectangles reflect better the areas of changes, but can also possibly mean more points in the final model/point-cloud. The selectively densified point-cloud, obtained by the addition of the high resolution data scanned over the regions framed in Fig. 6d to the initial growing neural gas map, is shown in Fig. 6e and contains in this case 3584 points.

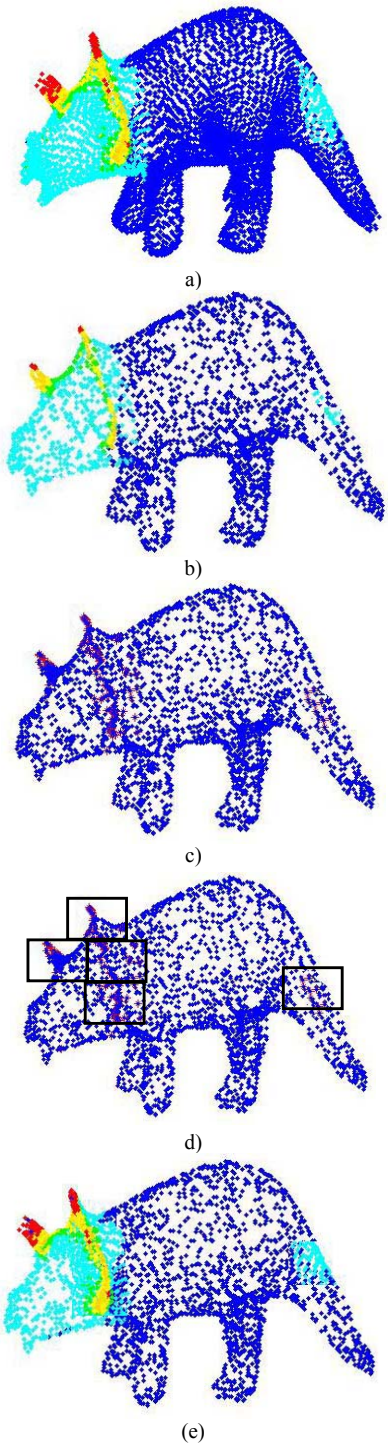

Fig. 6. (a) Initial scan of triceratops with compliance, b) growing neural gas model, c) remaining triangle vertices after removal procedure (shown in red), d) areas of elasticity change detected in the growing neural gas map, and e) growing neural gas map augmented with high resolution data from the selected regions.

This example demonstrates that the proposed method provides a significantly compressed model when compared to the initial scan that samples the entire surface without selectivity (about 95% reduction in the number of points from the full resolution scan of 65536 points).

V. Conclusions

The proposed framework can be used to automatically identify areas where changes in the elastic characteristics of an object occur starting from a sparse geometric scan enhanced with elasticity measures. The method works well on objects made from non-homogeneous materials, as well as in cases where the elastic behavior is not correlated with a change in the local geometry of the object, such as the case of the triceratops and the pliers. The obtained multi-resolution deformable model also significantly improves the compactness of the object's 3D geometric and elasticity characteristics.

Future research is dedicated to a coherent integration of the previously proposed 3D vision probing with the new elasticity data acquisition procedure to efficiently build multi-resolution deformable object models.

Acknowledgments

The authors want to thank Dr. Jochen Lang for making available the triceratops point-cloud and the force-displacement data.

References

[1] D. Aulignac, C. Laugier, and M.C. Cavusoglu, "Towards a Realistic Echographic Simulator with Force Feedback", *Proc. IEEE/RSJ Int. Conf. Intelligent Robots and Systems*, pp. 727-732, Kyongju, Korea, 1999.

[2] D. K. Pai, K. van den Doel, D. L. James, J. Lang, J. E. Lloyd, J. L. Richmond, and S. H. Yau, "Scanning Physical Interaction Behavior of 3D Objects", *Proc. Computer Graphics and Interactive Techniques,* pp. 87-96, 2001.

[3] J. Lang, D.K. Pai, and R. J. Woodham, "Acquisition of Elastic Models for Interactive Simulation", *Int. Journal of Robotics Research*, vol. 21, no.8, pp.713-733, 2002.

[4] A.-M. Cretu, J. Lang and E.M. Petriu, "Adaptive Acquisition of Virtualized Deformable Objects with a Neural Gas Network", *Proc. IEEE Int. Workshop Haptic Audio Visual Environments and their Applications*, Ottawa, Canada, pp.165-170, Oct. 2005.

[5] A.-M. Cretu, P. Payeur and E.M. Petriu, "Selective Vision Sensing with Neural Gas Networks", *Proc. IEEE Int. Instr. and Meas. Technology Conf.*, pp. 478-483, Victoria, Canada, May 2008.

[6] A.-M. Cretu, E.M. Petriu and P. Payeur, "Evaluation of Growing Neural Gas Networks for Selective 3D Scanning", *Proc. IEEE Int. Workshop on Robotic and Sensors Environments,* pp. 108-113, Ottawa, Canada, Oct. 2008.

[7] A.-M. Cretu, P. Payeur and E. M. Petriu, "Neural Network Mapping and Clustering of Elastic Behavior from Tactile and Range Imaging for Virtualized Reality Applications", *IEEE Transactions on Instrumentation and Measurement,* vol. 57, no 9, pp. 1918-1928, 2008.

[8] B. Fritzke, "Unsupervised Ontogenic Networks", in *Handbook of Neural Computation*, C2.4, Eds. E. Fiesler, R. Beale, IOP Publishing Ltd and Oxford University Press, 1997.

[9] T.M. Martinetz, "Competitive Hebbian Learning Rule Forms Perfectly Topology Preserving Maps", *Proc. of Int. Conf. Artificial Neural Networks,* Springer, Amsterdam, pp. 427-434, 1993.

[10] B. Fritzke, "Some Competitive Learning Methods", draft, 1997, [Online]. Available: http://www.neuroinformatik.ruhr-unibochum.de/ini/VDM/research/gsn/ JavaPaper